Supporting Information for

Influence of support morphology on the bonding of molecules to nanoparticles

Yim et al.

This supporting information provides Supporting Methods (Calculation Details, Analysis of μ-NEXAFS Data), and a figure showing large area STM images of the step-islands.

Supporting Methods

1. Calculation Details

DFT-vdW calculations were performed using the Vienna *ab initio* simulation package (VASP, version 5.2.12) with the projector-augmented wave (PAW) method and a cutoff of 500 eV for the plane wave expansion of the wave-functions (42, 43). For the exchange-correlation functional, we have used the optB86b vdW functional implemented in VASP by Klimés et al. (44), using the algorithm of Román-Pérez and Soler (45). A spin-restricted approach has been used as spin polarization effects have been found to be negligible. Geometry optimizations were performed on a super-cell structure using periodic boundary conditions. The (111) surface is modeled using a four-layer slab, with a CO adlayer on one side of the slab and a vacuum space equivalent to six ideal bulk metallic layers. We use the lattice constant of 3.946 Å, calculated theoretically for Pd, which is close to the experimental value of 3.891 Å. We calculated the average adsorption energies of CO molecules in three c(4×2)-2CO unit cells with different site occupations of CO: in the first unit cell CO occupies both atop and bridge sites (TB), in the second unit cell CO occupies only bridge sites (BB), and in the last unit cell CO occupies both fcc and hcp hollow sites (HH). Note that all these unit cells correspond to the same CO coverage of 0.5 ML. We also tested the stability of these different c(4×2)-2CO overlayers under anisotropic surface strain conditions. Tensile strain ($\varepsilon_s > 0$) is modeled by elongation along $\left[\bar{1}01\right]$ (see Fig. 5*B*) together with compression along $\left[\bar{1}2\bar{1}\right]$ and *vice versa* for compressive strain ($\varepsilon_s < 0$). The ratio between the compressed strain applied along one direction and the tensile strain applied along the other (orthogonal) direction is set at 0.39, equal to the Poisson ratio of bulk Pd. During the calculations, the CO molecules and the two

uppermost Pd substrate layers are allowed to relax, while the bottom two layers of Pd atoms are fixed in their bulk positions. All atomic coordinates of CO and Pd in the relaxed metal layers were optimized to a force of less than 0.01 eV/Å on each atom. Brillouin zone integration was performed using a Monkhorst-Pack grid of 4×4×1 for the c(4×2) unit cells, and a Methfessel-Paxton smearing of 0.2 eV. Adsorption energies are calculated by subtracting the total energy of the adsorption system from that of the separated molecule and metal slab, the latter is under the same strain condition as the adsorption system.

2. Analysis of μ-NEXAFS Data

The inset of Fig. 3*B* shows an XPEEM image of a TiO_2(110) surface following Pd deposition. The image was collected with an electron kinetic energy of 0.5 eV and photon energy of 430 eV. As this photon energy is above the Pd $M_{4,5}$ edges but still below the Ti $L_{2,3}$ edges, the bright feature in the image with a measured diameter of about 1.5 μm (circled) corresponds to a Pd nanoparticle, the dark background being the TiO_2(110) substrate (21). This surface was exposed to 120 L (1 L = 1.33×10^{-6} mbar.s) of CO *in-situ* at room temperature. According to our STM experience, this should lead to ~0.5 ML coverage of all the Pd nanoparticle facets (1 ML = 1.527×10^{15} molecules.cm^{-2}).

Carbon K-edge (hν = 285-293 eV) μ-NEXAFS measurements were recorded from this surface in order to determine the bond orientation of CO on the Pd nanoparticle. This was achieved by recording a series of XPEEM images in the same surface region with an electron kinetic energy of 2 eV and photon energies ramping between 285 and 293 eV.

By assuming that the location of the Pd nanoparticle in the field-of-view (FOV) in XPEEM does not change during the measurement, and by employing a data-mask, we extracted C K-edge X-ray absorption spectra from the Pd nanoparticle which are shown in Fig. 3*A*. The absorption peak at hν = 286.9 eV corresponds to the π* resonance of CO. This peak exhibits a strong dependence on the polarization angle, β, shown in the inset of Fig. 3*B*. β represents the orientation of the electric vector of the incident photon beam. When β is 0º, the electric vector of the photon beam lies in the plane of incidence and corresponds to *p*-polarized light. Note that the angle of incidence, θ, is always fixed at 16º. On the other hand, when β is 90º, the electric vector of the photon beam is perpendicular to the plane of incidence and corresponds to *s*-polarized light.

The areas of the π* resonance at different polarization angles were obtained by fitting the μ-NEXAFS curves in the vicinity of the π* peak with a Gaussian function, as shown in Fig. 3*B*. In order to determine the bond angle of CO relative to the top facet of the Pd nanoparticle, we numerically fitted the experimental data points in Fig. 3*B* using Equations S1 to S3 which are modified versions of those of Stöhr and Outka (31). This gives the polar bond angle of CO, γ, as 21.4˚ ± 7.0˚, very close to the value obtained in our previous measurements using conventional NEXAFS (26).

While the non-zero bond angle seems to imply that the CO bonds with its molecular axis off the (111) top facet normal, the situation is rather more complicated. A significant proportion of CO molecules adsorb on the side facets of the Pd nanoparticle and this must be accounted for. To do this, we simulated the μ-NEXAFS measurements on the basis that CO bonds with its molecular axis parallel to the facet normal. In the simulation, we observed that as the contribution of the side facets to the X-ray absorption signal becomes larger, the normalized π* peak area at β = 0˚

increases to higher values and so the apparent bond angle moves further from the (111) top facet normal.

Supporting Equations

$$I_p = B\left[\cos^2\beta I_p^{\parallel} + \sin^2\beta I_p^{\perp}\right] \tag{S1}$$

where

$$I_p^{\parallel} = \frac{2}{3}\left[1 - \frac{1}{4}\left(3\cos^2\theta - 1\right)\left(3\cos^2\gamma - 1\right)\right] \tag{S2}$$

and

$$I_p^{\perp} = \frac{1}{2}\left(1 + \cos^2\gamma\right) \tag{S3}$$

In Equations S1-S3, B is an arbitrary constant, β is the polarization angle of the photon beam, θ is the incident angle of the photon beam, and γ is the polar bond angle of CO relative to the surface normal of the (111) top facet.

Supporting Figures

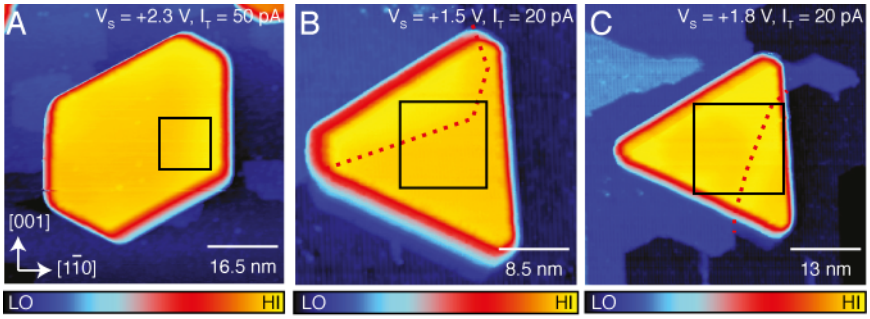

Fig. S1. Topographical STM images of Pd nanocrystals with curved (111) top-facet. (*A*) STM image (66 × 66 nm^2, 78 K) of the step-island shown in Fig. 2. A square marks the area on the top-facet from which Fig. 2*A* was taken. The color bar has a range of 5.56 nm. The scale bar is 16.5 nm. (*B*) STM image (34 × 34 nm^2, 124 K) of the step-island shown in Fig. 4. The red dashed line roughly indicates the location of the substrate step edge that lies beneath the island and the square marks the area on the top-facet where Fig. 4*A* was taken. The color bar has a range of 2.57 nm. The scale bar is 8.5 nm. (*C*) STM image (52 × 52 nm^2, 150 K) of the step-island shown in Fig. 6. The red dashed line roughly indicates the location of the substrate step edges that lies beneath the island and the square marks the area on the top-facet where Fig. 6*A* was taken. The color bar has a range of 2.72 nm. The scale bar is 13 nm. It is clear that the island grows across the steps in (*A*) and is curved as a result. However, because of the greater height of the island, it is difficult to mark the locations of the TiO_2(110) step-edges.